Search for Ξ^* resonances in 2.87-GeV/c K^-n interactions*

E. Briefel, S. A. Gourevitch, L. Kirsch, and P. Schmidt
Brandeis University, Waltham, Massachusetts 02154

C. Y. Chang, R. Staab, and G. B. Yodh
University of Maryland, College Park, Maryland 20742

R. Fernow,† P. Gauthier, G. Moneti, and M. Goldberg
Syracuse University, Syracuse, New York 13210

J. Canter, W. A. Mann, J. Schneps, J. Tompkins, and G. Wolsky‡
Tufts University, Medford, Massachusetts 02155
(Received 19 May 1975)

We report on a search for Ξ^* production in the mass range 1.5–2.0 GeV/c^2 in K^-n interactions at 2.87 GeV/c. Upper limits on Ξ^* production cross sections, as well as reaction cross sections for those final states in which Ξ^*'s may be observed, are presented. In particular, an upper limit of 5.4 μb is placed on production of an isospin-$\frac{3}{2}$ Ξ^{*--}.

I. INTRODUCTION

The understanding of excited Ξ states has proven to be a tantalizing[1] but elusive goal. The main interest in Ξ^* data lies in their application to the various classification schemes of elementary particles. The SU(3) framework predicts Ξ states as part of every baryon multiplet, often with predictable branching ratios.[2] On the other hand, exotic states have no place in the quark model, and it is of interest to establish their existence or at least upper limits on their production. In particular, K^-n interactions are well suited to a search for exotic Ξ^*'s because these can be produced in the quasi-two-body final state $\Xi^{*--}K^+$ which is not available in K^-p interactions. Finally, in the quark model SU(6)×O(3) symmetry scheme, experimental measurements can of course distinguish between different versions of the model.[3]

The experimental difficulties for Ξ studies are, however, well known. Complex final-state topologies have for the most part restricted investigations to the bubble chamber. In addition, the impossibility of formation experiments, production cross sections which decrease as $P_{\text{lab}}{}^{-4}$ from maxima of tens of microbarns, and multiple decay modes have resulted in low statistics with typically a few hundred or less events per final state.

The present experiment, which complements an earlier Brandeis-Maryland-Syracuse-Tufts (BMST) study of Ξ^* production by 2.9-GeV/c K^- in hydrogen,[4] is no exception. We have searched for Ξ^* production in the reactions

$$K^-n \to \Xi^{*-}K^0 , \tag{1a}$$

$$\to \Xi^{*--}K^+ , \tag{1b}$$

with

$$\Xi^* \to \Xi\pi ,$$

$$\to \Xi\pi\pi ,$$

$$\to \Xi(1530)\pi ,$$

$$\to \Lambda\bar{K} ,$$

$$\to \Sigma\bar{K}$$

initiated by 2.87-GeV/c K^- mesons incident upon a deuterium target. Our exposure amounts to ~16.5 events per microbarn, and spans the Ξ mass spectrum from 1.5 to 2.0 GeV/c^2. Although some evidence for excited Ξ^* structure exists in our data, we can report no statistically significant[5] signal in either the $I_z = \frac{1}{2}$ or the $I_z = \frac{3}{2}$ mass combinations, other than the well-established $\Xi^*_{1/2}(1530)$. We estimate an upper limit for the production of any Ξ^{*--} resonance, with a width < 60 MeV and a mass < 2.0 GeV/c^2, of 5.4 μb at the 90% confidence level. The lack of signal in Ξ^{*--} is consistent with the results of the one previous search for exotic Ξ resonances,[6] and establishes conclusively the $I = \frac{1}{2}$ assignment for the Ξ signals thus far observed[7] in the $\Xi\pi$ decay mode below a mass of 2 GeV/c^2.

The details of our experimental procedure will be given in Sec. II. Cross sections have been measured for all energetically available constrained states containing two visible signs of strangeness and are presented in Sec. III. Section IV contains the results of our search for Ξ structure in those channels.

II. EXPERIMENTAL DETAILS

The data for this experiment came from ~10^6 exposures of the deuterium-filled Brookhaven National Laboratory 31-in. bubble chamber to a separated beam of 2.87-GeV/c K^- mesons. The film was taken in six separate runs, with considerable variation in both beam and target purity. Beam K^- content was monitored with a threshold Čerenkov counter and later checked by an analysis of $K^- \to \pi^-\pi^-\pi^+$ decays. The results are shown in Table I, with an average beam purity of (76 ± 4)%. During the last three runs, the deuterium target was contaminated with substantial amounts of HD and H_2, effectively reducing our neutron target sensitivity. The target composition for each run is also listed in Table I.

The film was scanned twice in all three views for events with at least two visible decays of strange particles. To reduce the background of nonhyperon charged decays, each event was required to have one associated Λ or K^0. All candidates were measured on image plane and film plane measuring machines and processed through the geometric reconstruction and kinematic fitting programs TVGP and SQUAW. Each event was examined by a physicist at the scanning table. Events failing geometric reconstruction, and events with two or more apparent signs of strangeness but no successful fit (probability of 0.1% or greater) to an acceptable hypothesis were remeasured, reprocessed, and once more examined. At least two such passes were made. Events lacking two signs of strangeness were rejected. All events having successful fits were checked for consistency between the observed ionization of charged tracks and the ionization determined by the fit. Wherever possible, ambiguities were resolved using ionization criteria.

Our final sample of 4811 events (including those fitting only unconstrained missing-mass hypotheses) represents about 20% of the total number of candidates found in the scans. The rejected events consisted of unassociated neutral decays (38%), charged meson decays (18%), double-hyperon production (12%), γ rays (7%), or were either unmeasurable or π^- induced.

For convenience in subsequent discussions we define the following notation: A subscript 1 is used for particle decays with seen decay products such as $K_1^0 \to \pi^-\pi^+$ and $\Lambda_1 \to p\pi^-$, as well as Ξ_1^-, Ξ_1^0, and Σ_1^0, where the decay is accompanied by a Λ_1. A subscript 2 is used when the decay products are not observed.

In order to restrict our sample to K^-n interactions, we require the spectator proton to have a momentum of less than 200 MeV/c. The expected loss of events incurred by such a selection is 9% for the Hamada-Johnston[8] deuteron wave function, leading us to adopt a correction factor of 0.91 ± 0.04.[9] In approximately 70% of the events the spectator proton track is too short to be detected. Constrained fits with a missing proton were first tried. If none of these were successful, the events were then fitted by assigning momentum components $P_x = P_y = (0 \pm 30)$ MeV/c, $P_z = (0 \pm 50)$ MeV/c to the unseen spectator and treating it as a measured track. In Fig. 1 we show the combined spectator proton momentum distribution for a sample of events corresponding to final states which have a four-constraint fit at production with a seen spectator and a one-constraint fit with an unseen spectator. The shaded portion is the contribution from unseen spectators. The figure indicates that the impulse approximation is a reasonable assumption, and that events with seen and unseen protons are found and processed with equal efficiencies.

Because of the low numbers of events produced in experiments of this type, resolution of kinematic ambiguities is especially critical. After application of the spectator momentum cut, there is no ambiguity between neutron and proton target events—the final-state proton is always identifiable. Occasional double solutions in kinematic fitting, amounting to no more than 6% of the sample, were each given a weight of $\frac{1}{2}$. Ambiguities consisting of a choice between a four-constraint (4C) fit at production and a one-constraint (1C) fit were resolved by selecting the more highly constrained 4C fit.

The remaining ambiguities were found to be in two topologies, which consisted of the following

TABLE I. Beam and target composition.

Run	No. beam tracks	Beam K^- content (%)	Chamber liquid	Average no. neutrons/nucleus	Target density (g/cm^3)
I, II, III	4.70×10^6	82 ± 4	D_2	1.00	0.138 ± 0.002
IV	1.14×10^6	68 ± 9	$0.66D_2$ $0.27HD$ $0.07H_2$	0.80	0.121 ± 0.002
V	1.06×10^6	61 ± 5	$0.74D_2$ $0.23HD$ $0.03H_2$	0.86	0.127 ± 0.006
VI	1.89×10^6	78 ± 7	$0.70D_2$ $0.25HD$ $0.05H_2$	0.83	0.124 ± 0.002

reactions:

$$K^-d \to \Xi_2^- K_1^0 \pi^0 p_s \ , \quad (2a)$$

$$\to \Sigma^- K_1^0 K_2^0 p_s \ , \quad (2b)$$

$$K^-d \to \Xi_1^0 \pi^- K_1^0 p_s \ , \quad (3a)$$

$$\to \Lambda_1 K^- K_1^0 p_s \ , \quad (3b)$$

$$\to \Sigma_1^0 K^- K_1^0 p_s \ . \quad (3c)$$

There were 56 events ambiguous between reactions (2a) and (2b), as well as 61 events having reaction (3a) ambiguous with reaction (3b), (3c), or both, and an additional 36 events ambiguous between reactions (3b) and (3c). Ambiguities between reactions (3) and the final states $\Lambda_1 K^- K_1^0 \pi^0 p_s$ or $\Lambda_1 \pi^- K_1^0 K_2^0 p_s$ were few in number (17 events) and will not be considered further.

When the events ambiguous between reactions (2) are interpreted as $\Sigma^- K_1^0 K_2^0 p_s$ there is a very strong $\phi(1019)$ peak in the $K_1^0 K_2^0$ mass distribution. This is also a dominant feature of the unique $\Sigma^- K_1^0 K_2^0 p_s$ events. Furthermore, interpreting the ambiguous events as $\Sigma^- K_1^0 K_2^0 p_s$ leads to a production angular distribution of the Σ^- with a strong peak consistent with meson exchange, whereas interpretation as $\Xi_2^- K_1^0 \pi^0 p_s$ yields a Ξ^- production angular distribution which disagrees strongly with that observed for unambiguous Ξ^- events and with expectations for baryon exchange. On the basis of this evidence we assign the entire ambiguous sample to the final state $\Sigma^- K_1^0 K_2^0 p_s$.

The Ξ_1^0, Λ_1, Σ_1^0 ambiguities of reactions (3) present a more difficult separation problem. We have proceeded by first identifying the Ξ_1^0 content of the ambiguous sample, and then treating the Λ-Σ^0 case. If the three final states mentioned are treated generically as

$$K^-d \to m^- K_1^0 \Lambda_1 X^0 p_s \quad (4)$$

($X^0 = \pi^0$, 0, or γ; $m^- = \pi^-$ or K^-), and if we use the fact that the decay distributions for true $\Xi^0 \to \Lambda\pi^0$ and $\Sigma^0 \to \Lambda\gamma$ decay should be isotropic, then the measured center-of-mass decay distribution $\cos\theta^*$ of the Λ in the (ΛX^0) system provides Ξ^0 discrimination. Interpreting m^- as π^- $(\cos\theta_\pi^*\text{-})$ this distribution will be uniform for Ξ^0 and peaked forward for Λ, Σ^0. Interpreting m^- as K^- $(\cos\theta_K^*\text{-})$ this distribution will be peaked backward for Ξ^0, uniform for Σ^0, and forward for Λ. In Fig. 2 we show the two distributions projected from the corresponding two-dimensional plot. The peak of Λ, Σ^0 is evident in $\cos\theta_\pi^*$-, along with a uniform background of Ξ^0 which reflects as a backward peak in $\cos\theta_K^*$-. We identify the events with $\cos\theta_K^*\text{-} < -0.6$ as Ξ^0, the remainder as Λ or Σ^0.

Standard missing-mass and momentum techniques have been found to be incapable of providing discrimination between reactions (3b) and (3c). The Λ-Σ^0 separation has been effected by examining the fitted Σ^0 center-of-mass decay angle $\hat{\Sigma}^0 \cdot \hat{\Lambda}$. True Λ events fitting the Σ^0 hypothesis will be peaked forward in $\hat{\Sigma}^0 \cdot \hat{\Lambda}$, as is evident in Fig. 3. Identifying the events with $\hat{\Sigma}^0 \cdot \hat{\Lambda} > 0.7$ as Λ, we esti-

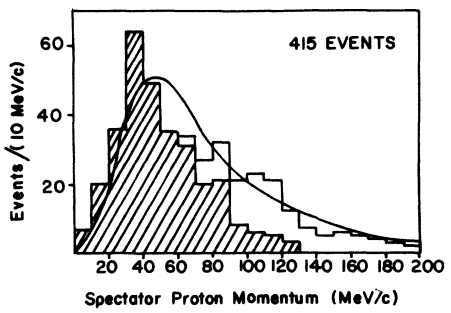

FIG. 1. Spectator-proton momentum distribution for the final states $\Xi_1^- K_1^0$, $\Xi_2^- K_1^0$, $\Xi_1^- \pi^- K^+$, $\Lambda_1 K^- K_1^0$, and $\Sigma^- K_1^0 K_1^0$. Unseen spectators are shown shaded. Solid curve is the normalized Hamada-Johnston distribution.

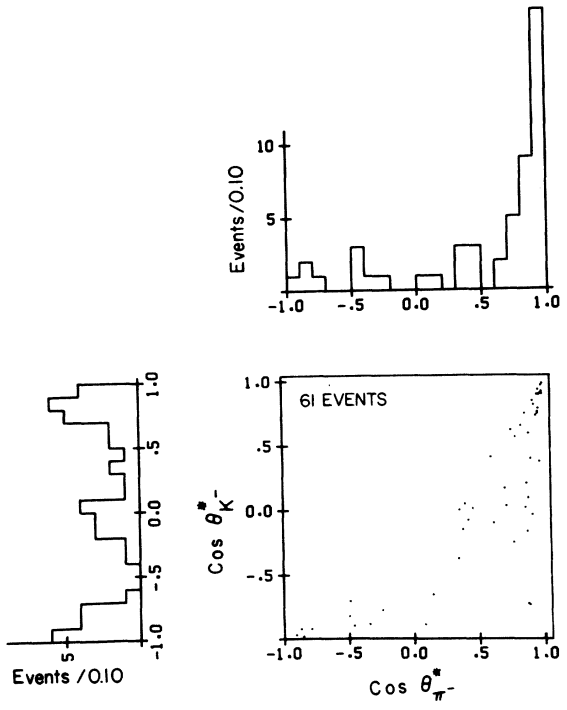

FIG. 2. Diplot and projections of the measured center-of-mass decay angular distribution of the Λ in the ΛX^0 system, for events ambiguous between Ξ^0 and Λ or Σ^0. Events with $\cos\theta_K^*\text{-} < -0.6$ are identified as Ξ^0.

mate a Σ^0 contamination of the Λ sample in any final state to be less than 7%.

The few remaining unresolvable ambiguities have been assigned equally to the competing hypotheses. Their effect on the results discussed in the following sections is negligible.

III. CROSS SECTIONS

The cross section for each channel is computed from

$$\sigma = N_{\text{corr}}/E ,$$

where N_{corr} is the number of events observed and then corrected for geometric cuts, scanning efficiency, processing efficiency, probability cutoff, spectator momentum cut, kinematic ambiguities, and visibility factors for neutral decays. The determination of these factors will be discussed in subsequent paragraphs. The sensitivity E, which is a measure of the beam particle flux reaching the target nucleon, is defined as

$$E = L \times n_t \times 1/G ,$$

where L is the effective path length of the K^- beam, n_t is the target density in neutrons or protons per cm^3, and $G = 1.05 \pm 0.02$ is the Glauber correction[10] which accounts for shadowing of the target nucleon in the deuterium. The path length L has been determined by a count of K^- entering our fiducial volume (of length 64.0 cm in the beam direction) and has been corrected for beam curvature and for attenuation of the beam by interaction and decay. The density n_t, which is different for neutrons and protons in this experiment due to the presence of target contaminants, was determined by measurement of the range of μ^+ from stopping π^+ and by mass spectrographic analysis of the target composition (see Table I).

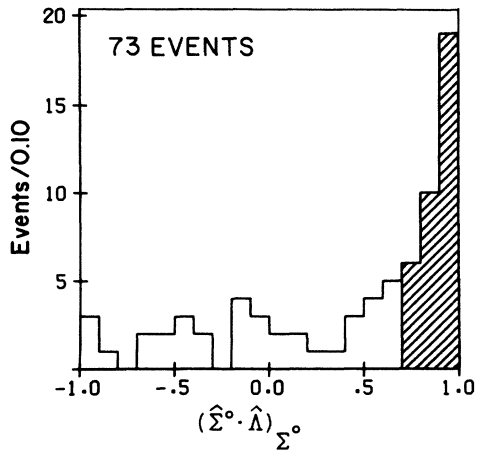

FIG. 3. Fitted Σ^0 center-of-mass decay angle, for events ambiguous with Λ. Shaded portion represents the forward Λ peak.

The sensitivity of our entire exposure amounts to 16.5 events per microbarn for K^-n interactions and 17.9 events per microbarn for K^-p interactions. A portion of the film corresponding to 14.6 $\pm$0.35 events per microbarn has been used for the K^-n cross-section determinations.

It is well known that the standard Geiger-Werner technique[11] for calculating scanning efficiency from two separate scans can yield a severe overestimate because it is based upon the assumption that all events of a certain topology have an equal probability of being observed. Such an assumption is likely to be very much in error in this type of experiment given the complex configurations of events with two visible signs of strangeness. Various studies done in this experiment, and in the previous BMST hydrogen experiment, consisting of careful third scans and analysis with the visibility-dependent Derenzo-Hildebrand technique,[12] show that a reasonable value for the scanning efficiency is (84 $\pm$7)%.

Our processing efficiency has been computed from the small fraction of events which cannot be classified as good or as rejects after several passes through the processing-editing procedure, and from the numbers of total and good events in each of two passes. We obtain an average processing efficiency of (91.5 $\pm$2.5)%.

The net correction factor for the effect of the scanning and processing efficiencies, probability cut, spectator momentum cut, and loss of events near the beam entrance window is 1.50 $\pm$ 0.16. Further channel-dependent correction factors account for ambiguity assignments and geometric detection efficiencies. The geometric weighting procedure follows that adopted for the previous BMST K^-p experiment.[13]

Table II contains our results for all channels having a fully corrected cross section (including visibility factors) of 1.0 μb or greater. The final-state cross sections derived from different topologies (such as $\Xi^-K^0\pi^0$ from $\Xi_1^-K_1^0\pi^0$ and $\Xi_2^-K_1^0\pi^0$) agree within the errors, with one serious exception. There appears to be a significant loss of $\Xi_1^-K_1^0$ events compared to $\Xi_1^-K_2^0$ and $\Xi_2^-K_1^0$ (see Table II). This could be due to two causes: difficulties in fitting this highly constrained topology, or a reduced scanning efficiency for finding all three signs of strangeness. In the latter case, true $\Xi_1^-K_1^0$ events will be included in the $\Xi_1^-K_2^0$ and $\Xi_2^-K_1^0$ samples, inflating these measured cross sections. We can compute the number of events which would have to be redistributed among the

TABLE II. Cross sections.

Topology	No. of events [a]	Weighted no. of events	Topological cross section (μb)	Reaction final state	Cross section (μb) [c]
$\Xi_1^-K_1^0$	25(0)	24 ±9	2.5 ±0.9 [d]	Ξ^-K^0	11.1 ±4.2 [d]
$\Xi_1^-K_2^0$	134(0)	240 ±25	24.6 ±3.6	Ξ^-K^0	55.4 ±8.1
$\Xi_2^-K_1^0$	49(0)	49 ±9	5.0 ±1.1	Ξ^-K^0	45.3 ±9.5
$\Xi_1^-K_1^0\pi^0$	53(0)	70 ±12	7.2 ±1.4	$\Xi^-K^0\pi^0$	32.4 ±6.3
$\Xi_2^-K_1^0\pi^0$	59(0)	48 ±8	4.9 ±1.0	$\Xi^-K^0\pi^0$	44.1 ±8.6
$\Xi_1^-K^+\pi^-$	218(0)	305 ±24	31.3 ±4.1	$\Xi^-K^+\pi^-$	47.0 ±6.1
$\Xi_1^0K_1^0\pi^-$	96(7)	122 ±16	12.5 ±2.1	$\Xi^0K^0\pi^-$	56.3 ±9.5
$\Xi_1^-K^+\pi^-\pi^0$	61(10)	76 ±12	7.8 ±1.5	$\Xi^-K^+\pi^-\pi^0$	11.7 ±2.2
$\Xi_1^-K_2^0\pi^-\pi^+$	60(10)	65 ±10	6.6 ±1.3	$\Xi^-K^0\pi^-\pi^+$	15.0 ±2.9
$\Xi_2^-K_1^0\pi^-\pi^+$	21(0)	24 ±6	2.4 ±0.7	$\Xi^-K^0\pi^-\pi^+$	21.8 ±6.2
$\Xi_2^-K_1^0\pi^-\pi^+\pi^0$	4(0)	5 ±3	0.53 ±0.31	$\Xi^-K^0\pi^-\pi^+\pi^0$	4.8 ±2.8
$\Lambda_1K^-K_1^0$	64(3)	72 ±10	7.4 ±1.2	ΛK^-K^0	33.2 ±5.4
$\Lambda_1K^-K_1^0\pi^0$	19(7)	15 ±4	1.6 ±0.5	$\Lambda K^-K^0\pi^0$	7.1 ±2.2
$\Lambda_1K_1^0K_1^0\pi^-$	2(0)	3.7 ±2.7	0.38 ±0.28		
$\Lambda_2K_1^0K_1^0\pi^-$	6(3)	4.0 ±2.3	0.41 ±0.24		
$\Lambda_1K_1^0K_2^0\pi^-$	126(10)	123 ±13	12.7 ±1.9		
$\Sigma^-K_1^0K_1^0$	24(0)	19 ±6	1.91 ±0.65		
$\Sigma^-K_1^0K_2^0$	268(0)	316 ±22	32.5 ±4.1		
$\Sigma_1^0K^-K_1^0$	48(3)	58 ±9	6.0 ±1.1	$\Sigma^0K^-K^0$	26.9 ±5.0
$\Sigma^-K^-K_1^0\pi^+$	5(1)	5 ±3	0.52 ±0.28	$\Sigma^-K^-K^0\pi^+$	1.6 ±0.9
$\Sigma^-K^+K_1^0\pi^-$	6(1)	7 ±3	0.74 ±0.36	$\Sigma^-K^+\bar{K}^0\pi^-$	2.2 ±1.1
$\Sigma^+K^-K_1^0\pi^-$	4(0)	8 ±5	0.85 ±0.52	$\Sigma^+K^-K^0\pi^-$	2.6 ±1.6

[a] Total number of events (number of unresolved ambiguities).
[b] Corrected for geometric detection efficiency and ambiguities.
[c] Corrected for neutral decays.
[d] Cross section not reliable (see text).

three topologies in order to give equal final-state cross sections; we find the measured $\Xi_1^-K_2^0$ cross section given in Table II would have to be reduced by about 2 standard deviations, and that of the $\Xi_2^-K_1^0$ reduced by about 1 standard deviation. These constitute the *maximum* effect on the $\Xi_2^-K_1^0$ and $\Xi_1^-K_2^0$ cross sections if reduced scanning efficiency for three signs of strangeness were the only cause of depletion of $\Xi_1^-K_1^0$ events. However, as evidence against this hypothesis, we note that any depletion of $\Xi_1^-K_1^0\pi^0$ events relative to $\Xi_2^-K_1^0\pi^0$ is much smaller, being about 1 standard deviation. Further, in support of the assumption of fitting difficulties, we find among the sample of rejected events about 50 which appear to have three signs of strangeness and yet do not fit after several measurements. At least some of these are certain to be good events. In view of these arguments, we conclude that the $\Xi_1^-K_2^0$ and $\Xi_2^-K_1^0$ cross-section measurements are reasonably reliable, but that the $\Xi_1^-K_1^0$ is not, and quote the latter for comparison only.

As a further check on our procedure, we have measured the cross sections for the constrained reactions $K^-p \to \Xi_1^-K^+$ and $K^-p \to \Xi_2^-\pi^+K_1^0$ for comparison with the corresponding cross sections found in the previous hydrogen experiment. For this experiment we obtain 26.1 ±3.3 and 8.7 ±1.4 μb, respectively, before correction for neutral decays. These are in good agreement with the hydrogen values of 23.1 ±2.7 and 7.3 ±1.0 μb.

IV. SEARCH FOR Ξ* PRODUCTION

Presented below are the results of our search for evidence of Ξ* structure in those final states in which production of either an $I=\frac{1}{2}$ or an $I=\frac{3}{2}$ Ξ* is possible. The discussion is limited to those channels with sufficient statistics for meaningful analysis.

(a) $K^-n \to \Xi^-\pi^-K^+$. The three mass projections for the 238 events in this channel are shown in Fig. 4. The data have been fitted using the maximum-likelihood method to $K^*(890)$ production and phase space, and found to contain (51 ± 7)% $K^-n \to \Xi^-K^{*0}(890)$. The shaded area in $M(\Xi^-\pi^-)$ represents the events remaining after removal of the events in the mass interval $0.84 \leq M(K^+\pi^-) \leq 0.94$ GeV/c^2. The upper curve corresponds to the fitted distribution and the lower curve is phase space normalized to the shaded events. The three peaks in $M(\Xi^-\pi^-)$ all have a significance of less than 3 standard deviations. Also, the distributions of the center-of-mass production angle of the $\Xi^-\pi^-$ system show no variation between the peak and other regions. We conclude that there is no strong evidence for production of a Ξ^{*--}, and place an upper limit of 4.7 μb on the production of a Ξ^{*--} with width less than 40 MeV and mass less than 2 GeV/c^2, with 90% confidence.[14]

(b) $K^-n \to \Xi^-\pi^0K_1^0$, $\Xi^0\pi^-K_1^0$. Figure 5 contains the

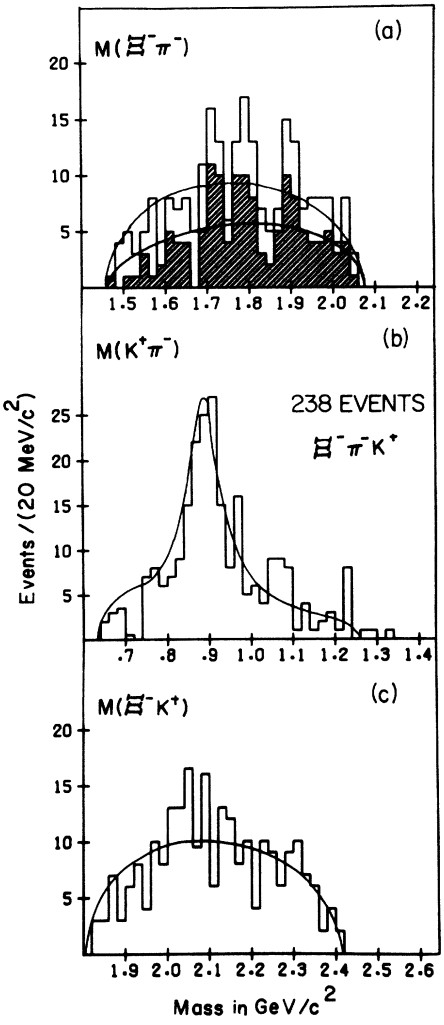

FIG. 4. Effective-mass distributions for the final state $\Xi^-\pi^-K^+$. (a) $M(\Xi^-\pi^-)$. (b) $M(K^+\pi^-)$. (c) $M(\Xi^-K^+)$. Shaded area in (a) represents the 134 events remaining after removal of events in the $K^{*0}(890)$ mass region. The lower curve in (a) is phase space normalized to the shaded events. The upper curve in (a) and the curves in (b) and (c) represent a fit to 51% $\Xi^-K^{*0}(890)$ production plus phase space.

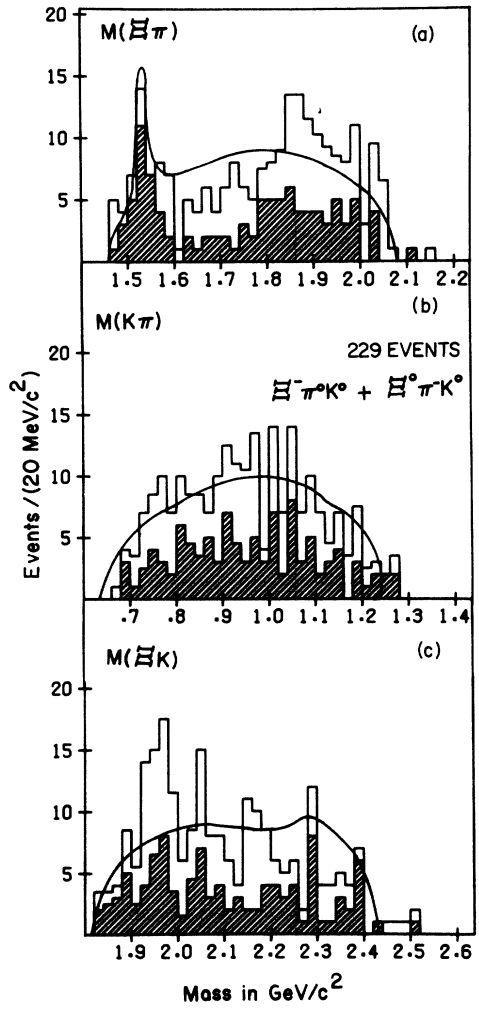

FIG. 5. Effective-mass distributions for the final states $\Xi^-\pi^0K_1^0$ (124 events) and $\Xi^0\pi^-K_1^0$ (105 events). Shaded part is the $\Xi^0\pi^-K_1^0$ contribution. (a) $M(\Xi\pi)$. (b) $M(K\pi)$. (c) $M(\Xi K)$. Solid curve represents unfitted distribution corresponding to 10% Ξ* (1530) production (see text).

combined mass distributions for these two final states, with the $\Xi^0\pi^-K_1^0$ contribution shaded. The only obvious resonant structure is $\Xi^{*-}(1530)$. The high-mass peaking in $\Xi\pi$ is consistent with previous experiments where Ξ resonances near masses of 1800 and 1930 MeV/c^2 have been observed. There also appears to be a sharp peak in $M(\Xi K)$ in the interval $1.92 \leq M(\Xi K) \leq 2.0$ GeV/c^2, evident in both the $\Xi^0\pi^-K^0$ and $\Xi^-\pi^0K^0$ final states [Fig. 5(c)]. The fit for these states is improved when a Σ^*, with a mass of about 1960 MeV/c^2, is included.[15] Also, the combined ΞK production angular distribution, shown in Fig. 6, does contain some backward peaking such as one would expect from a meson exchange process. However, the signal in Fig. 5(c) is of less than 3 standard-deviation significance, and no structure near $M(\Xi K)$ of 1960 MeV/c^2 is observed in the $\Xi^-\pi^-K^+$ final state [Fig. 4(c)] where, by isospin and visibility considerations, there should be a signal as large as that seen in $\Xi^-\pi^0K_1^0$. Since the high-mass $\Xi\pi$ and low-mass ΞK regions are correlated kinematically, we prefer to interpret the ΞK peak near 1960 MeV/c^2 as a reflection of known higher-mass $\Xi\pi$ effects.

There has been considerable interest in the $\Xi\pi$ mass region near 1630 MeV/c^2, with contradicting experimental claims and denials of a resonant state,[16] as well as theoretical predictions within the SU(6)×O(3) symmetry scheme.[3] No such signal is seen here in the $(\Xi\pi)^-$ mass spectrum. In order to measure an upper limit we keep in mind the difficulty in interpreting these final states, and use phase space normalized to the region $1.60 \leq M(\Xi\pi) \leq 1.78$ GeV/c^2 as our background. We find an upper limit of 2.7 μb for production of $\Xi^*(1630)$ in the region $1.60 \leq M(\Xi\pi) \leq 1.66$ GeV/c^2 at the 90% confidence level. By extending the same phase-space background to the high mass $\Xi\pi$ region, we can also measure the cross section corresponding to the excess of events in the interval $1.82 \leq M(\Xi\pi) \leq 1.94$ GeV/c^2. We obtain 14 μb. This number represents a maximum since a Σ^* (1960) reflection would enhance the apparent number of Ξ^* events.

(c) $K^-n \to \Xi_1^-\pi^-\pi^0K^+$. As is evident from the $\Xi^-\pi^0$ and $K^+\pi^-$ mass projections of Fig. 7 this final state is dominated by production of $\Xi^{*-}(1530)$ and $K^{*0}(890)$. A fit to the data yields $(29 \pm 12)\%$ $K^-n \to \Xi^{*-}K^{*0}$; $(24 \pm 14)\%$ $K^-n \to \Xi^-\pi^0K^{*0}$; and $(2 \pm 9)\%$ $K^-n \to \Xi^{*-}K^+\pi^-$. There is no evidence for production of higher mass Ξ^* states decaying into $\Xi^-\pi^0$.

The distribution in $M(\Xi^-\pi^-)$ for those events remaining after removal of the contribution from $\Xi^{*-}(1530) \to \Xi^-\pi^0$ and $K^{*0}(890) \to K^+\pi^-$ is shown in Fig. 8(a). No significant structure is evident. Figure 8(b) contains the $\Xi^-\pi^-\pi^0$ effective-mass distribution after removal of events involving $K^*(890)$ $[0.84 \leq M(K^+\pi^-) \leq 0.94]$. The shaded events represent those having $1.52 \leq M(\Xi^-\pi^0) \leq 1.58$ GeV/c^2. Again no evidence is apparent for production of Ξ^{*--}. We place an upper limit of 1.4 μb (90% confidence level) on production of a $\Xi^{*--} \to \Xi^-\pi^-\pi^0$ with width less than 40 MeV.

(d) $K^-n \to \Xi^-\pi^-\pi^+K^0$. The outstanding feature of this final state is that $(46 \pm 8)\%$ is produced in asso-

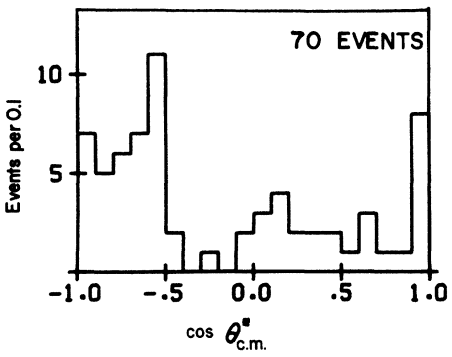

FIG. 6. Center-of-mass production angle of the ΞK system for events with $1.90 \leq M(\Xi K) \leq 2.02$ GeV/c^2 in the final states $\Xi^-\pi^0K^0$ and $\Xi^0\pi^-K^0$.

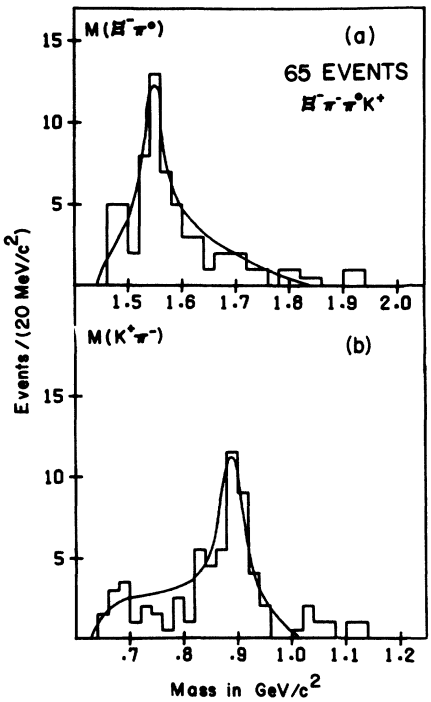

FIG. 7. Effective-mass distributions for the final state $\Xi^-\pi^-\pi^0K^+$. (a) $M(\Xi^-\pi^0)$. (b) $M(K^+\pi^-)$.

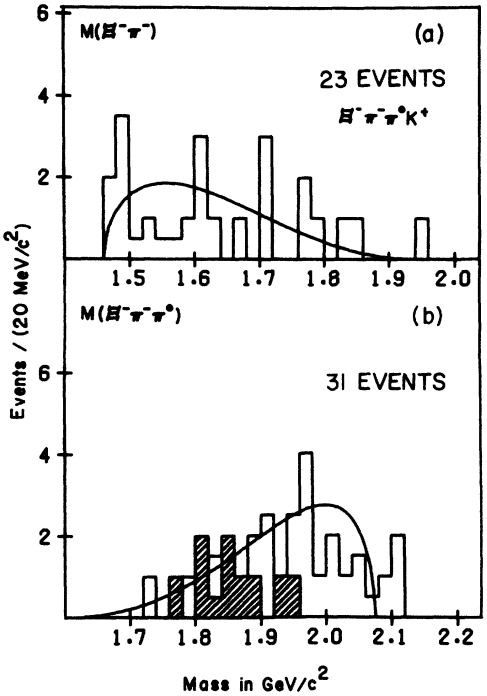

FIG. 8. Final state $\Xi^-\pi^-\pi^0K^+$. (a) $\Xi^-\pi^-$ effective-mass distribution after removal of events involving $\Xi^{*-}(1530)$ or $K^{*0}(890)$. (b) $\Xi^-\pi^-\pi^0$ effective-mass distribution after removal of events involving $K^{*0}(890)$. Shaded portion represents those events involving $\Xi^*(1530)$.

ciation with $\Xi^{*0}(1530)$, as may be seen in Fig. 9 where the $\Xi^-\pi^+$ effective mass is displayed. Although the statistics are quite low, the $\Xi^0(1530)\pi^-$ combined mass distribution of Fig. 10 shows some evidence for decay of $\Xi^{*-}(1820)$ into $\Xi(1530)\pi$, as

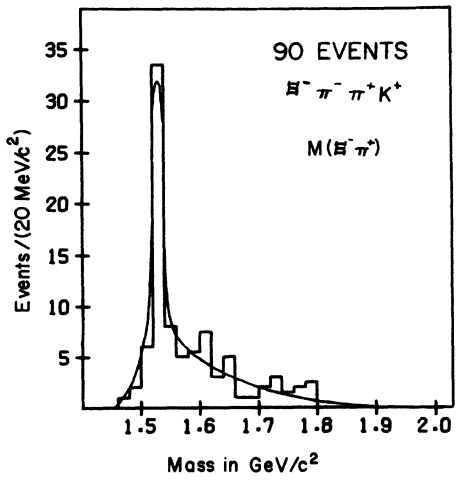

FIG. 9. $\Xi^-\pi^+$ effective-mass distribution for the final state $\Xi^-\pi^-\pi^+K^0$. Solid curve represents fit to 46% $\Xi^{*0}(1530)\pi^-K^0$ and 54% phase space.

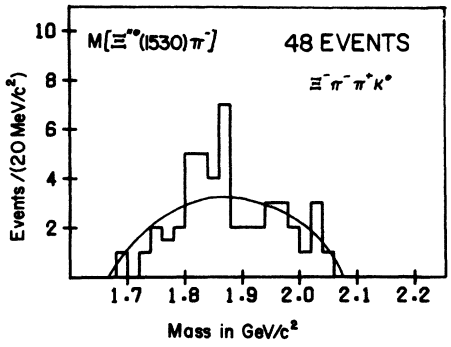

FIG. 10. $\Xi^{*0}(1530)\pi^-$ effective-mass distribution for the final state $\Xi^-\pi^-\pi^+K^0$. Solid curve represents expected distribution for 85% $\Xi^{*0}(1530)$ and 15% phase space in the mass interval $1.50 \leq M(\Xi^-\pi^+) \leq 1.56$ GeV/c^2.

has been observed previously in $\Xi\pi\pi K$ final states produced in K^-p interactions.[4] There is, however, no evidence for $\Xi^{*-}(1930) \to \Xi^{*0}(1530)\pi^-$. We estimate an upper limit of 1.9 μb at the 90% confidence level for the process $K^-n \to \Xi^{*-}(1930)K^0$, $\Xi^{*-}(1930) \to \Xi^{*0}(1530)\pi^-$.

Figure 11 contains the $I=\frac{3}{2}$ $\Xi^-\pi^-$ spectrum for this final state after removal of events having $\Xi^{*0}(1530) \to \Xi^-\pi^+$. The solid curve represents a normalized phase-space distribution. The region $1.60 \leq M(\Xi^-\pi^-) \leq 1.66$ GeV/c^2 yields an upper limit of 5.4 μb (90% confidence level) on production of an exotic Ξ^{*--} decaying into $\Xi^-\pi^-$.

(e) $K^-n \to \Lambda K^-K_1^0$. The reaction $K^-n \to \Lambda K^-K^0$ is expected to be very promising for analysis of $\Xi^* \to \Lambda\bar{K}$ decay because, unlike the corresponding proton target final state $\Lambda K^0\bar{K}^0$, it does not suffer from competing ϕ meson production or from our inability to distinguish $\bar{K}^0$ from K^0 decay. Figure 12 contains the ΛK^- effective-mass distribution for the 69 events remaining after ambiguity reso-

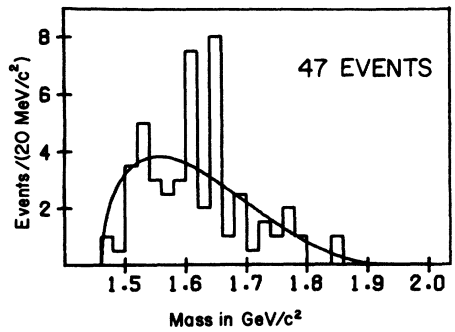

FIG. 11. $\Xi^-\pi^-$ mass distribution for the final state $\Xi^-\pi^-\pi^+K^0$ after removal of events with $\Xi^{*0}(1530) \to \Xi^-\pi^+$.

lution. There are 29 events (42% of the total) clustered in the mass region $1.78 \leq M(\Lambda K^-) \leq 1.86$ GeV/c^2, centered on 1820 MeV/c^2, and the Chew-Low plot of Fig. 13 indicates that they are produced preferentially with small momentum transfer (forward in the over-all center-of-mass system). It would appear that we are observing production and decay of $\Xi^{*-}(1820)$, although a fit to the data yields only $(18 \pm 7)\%$ $\Xi^*(1820)K^0$. However, the fitted background under the $\Xi^*(1820)$ is very likely increased by an excess of events near the upper end of phase space $[1.96 \leq M(\Lambda K^-) \leq 2.02$ GeV/$c^2]$ which may be the manifestation of a higher mass resonance. For the mass and width of $\Xi^*(1820)$ we obtain 1821 ± 3 MeV/c^2 and 16 ± 11 MeV, respectively. These may be compared with the values obtained for signals observed in the BMST hydrogen experiment[4]: 1871 ± 11 MeV/c^2 and 58 ± 39 MeV in $\Lambda K^0 \overline{K}^0$; 1854 ± 12 MeV/c^2 and 56 ± 14 MeV in $K^+\Sigma^-\overline{K}^0$; 1820 ± 12 MeV/c^2 and 82 ± 42 MeV in $\Xi(1530)\pi K$, and 1795 ± 10 MeV/c^2 and 99 ± 31 MeV in $\Xi^-\pi^+K^0$.

We obtain a cross section of 5.9 ± 2.5 μb for the process $K^-n \to \Xi^{*-}(1820)K^0$, $\Xi^{*-}(1820) \to \Lambda K^-$. Since this is based upon a fit which appears to underestimate the amount of $\Xi(1820)$ production, it should be considered as a lower limit. The paucity of data prevents more detailed analysis, such as spin-parity study using the Λ as a polarization analyzer.

(f) $K^-n \to \Sigma^-K_1^0K_2^0$. As is evident in the Dalitz plot of Fig. 14 and the mass projections of Fig. 15, this final state is strongly dominated by quasi-two-body production of $\phi(1019)$. A fit to the data yields $(58 \pm 4)\%$ $\Sigma^-\phi$ production, corresponding to a $\Sigma^-\phi$ production cross section of 82 ± 10 μb after correction for alternate decay modes of $\phi(1019)$. Since the strangeness -2 final-state mass combination is not unique, we have attempted to enhance any possible Ξ^* relative to background in the Σ^-K^0 spectrum by the center-of-mass production angle selection $\hat{K}^- \cdot \hat{K}^0 > 0$. This is based upon our expectation of baryon exchange for Ξ^* production. Figure 16 contains the combined Σ^-K^0 effective-mass distribution for the final states $\Sigma^-K_1^0K_1^0$ (29 events) and $\Sigma^-K_1^0K_2^0$ (323 events), with the $\phi(1019)$ events $[M(K_1^0K_2^0) \leq 1.05$ GeV/$c^2]$ removed from the latter, and with the above selection of the forward K^0 applied. No significant Ξ^* signal is observed. We find upper limits on the cross sections for production of $\Xi^{*-}(1820)$ and $\Xi^{*-}(1930)$ in the $\Sigma^-K^0\overline{K}^0$ final state of 4.3 μb and 4.5 μb, respectively, at the 90% confidence level.

(g) $K^-n \to \Lambda\pi^-K_1^0K_2^0$. The relevant mass distributions for this channel are shown in Fig. 17. Quasi-two-body $\Sigma^-(1385)$ $\phi(1019)$ production accounts for $(56 \pm 9)\%$ of the 139 events in this final state, corresponding to a cross section of 48 ± 14 μb after correction for alternate decay modes of the two resonant states. The ΛK^0 spectrum shows no evidence of Ξ^* structure.

V. CONCLUSIONS

We have performed a search for Ξ resonant states produced in K^-n interactions at 2.87 GeV/c with a sensitivity of ~16.5 events/μb. With the exception of the usual high-mass $(1.8 \to 2.0$ GeV/$c^2)$ peaking in the nonexotic $\Xi\pi$ mass spectrum from the $\Xi\pi K$ final states, the $\Xi K + \pi$'s channels exhibit little evidence of higher-mass Ξ^* production at the statistical level available in this experiment. The $\Xi^-\pi^-$ mass spectrum from the $\Xi^-\pi^-K^+$ final state contains three peaks of less than 3 standard-

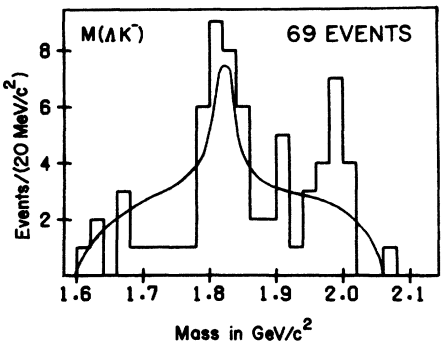

FIG. 12. ΛK^- effective-mass distribution for the final state $\Lambda K^-K_1^0$. Solid curve represents the fit containing 18% $\Xi^{*-}(1820)K^0$, plus phase space.

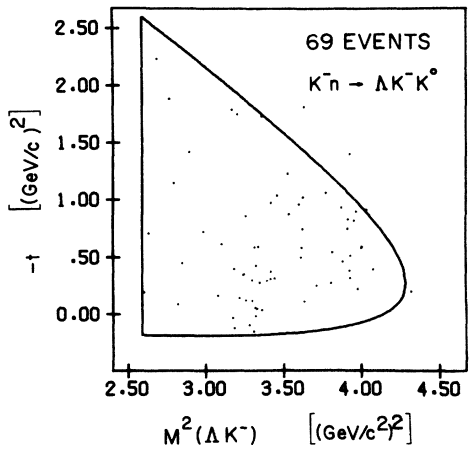

FIG. 13. Chew-Low plot for the ΛK^- system in the final state ΛK^-K^0.

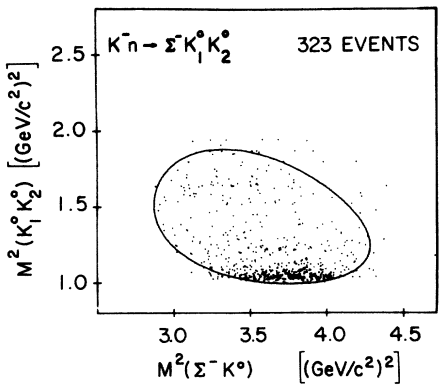

FIG. 14. Dalitz plot for the final state $\Sigma^- K_1^0 K_2^0$.

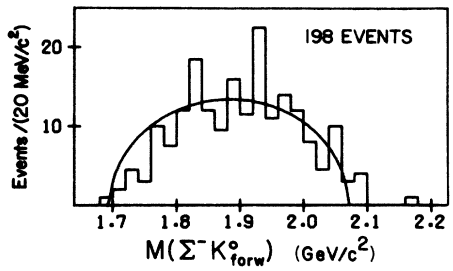

FIG. 16. $\Sigma^- K^0_{forw}$ effective-mass distribution, after removal of $\phi(1019)$ and selection of forward K^0, for the final states $\Sigma^- K_1^0 K_2^0$ and $\Sigma^- K_1^0 K_1^0$.

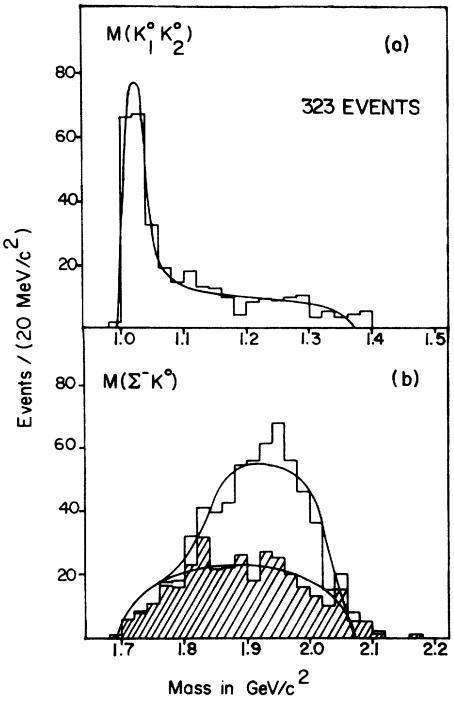

FIG. 15. Effective-mass distributions for the final state $\Sigma^- K_1^0 K_2^0$. (a) $M(K_1^0 K_2^0)$. (b) $M(\Sigma^- K^0)$. Solid curve on (a) and upper curve on (b) represent a fit to 58% $\Sigma^- \phi(1019)$ plus phase space. Shaded area of (b) represents events remaining after removal of $\phi(1019)$, and lower curve is phase space normalized to these events.

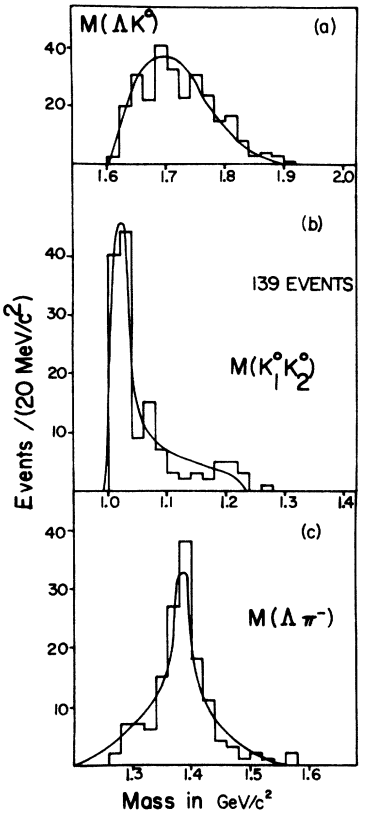

FIG. 17. Effective-mass distributions for the final state $\Lambda\pi^- K_1^0 K_2^0$. (a) $M(\Lambda K^0)$. (b) $M(K_1^0 K_2^0)$. (c) $M(\Lambda\pi^-)$.

TABLE III. Cross-section upper limits. All upper limits are at the 90% confidence level. See Ref. 14 for a description of the method used.

Process	Width (MeV)	Cross section (μb)
$K^-n \to \Xi^{*--}K^+$, $\Xi^{*--} \to \Xi^-\pi^-$	<40	<4.7
$K^-n \to \Xi^{*--}K^+$, $\Xi^{*--} \to \Xi^-\pi^-\pi^0$	<40	<1.4
$K^-n \to \Xi^{*--}\pi^+K^0$, $\Xi^{*--} \to \Xi^-\pi^-$	<60	<5.4
$K^-n \to \Xi^{*-}(1630)K^0$, $\Xi^{*-}(1630) \to \Xi\pi$	<60	<2.7
$K^-n \to \Xi^{*-}(1930)K^0$, $\Xi^{*-}(1930) \to \Xi^{*0}(1530)\pi^-$	<80	<1.9
$K^-n \to \Xi^{*-}(1820)K^0$, $\Xi^{*-}(1820) \to \Sigma^-\bar{K}^0$	<60	<4.3
$K^-n \to \Xi^{*-}(1930)K^0$, $\Xi^{*-}(1930) \to \Sigma^-\bar{K}^0$	<60	<4.5

deviation significance. While they cannot be considered evidence for production of an exotic resonance, they do increase the upper limit by about a factor of 2.5 from what it would have been for a smooth background. Finally, a promising reaction for further study with a high-statistics experiment is $K^-n \to \Lambda K^-K^0$, where we do find evidence for production of $\Xi^*(1820)$.

Table III represents a summary of our measured upper limits for production of both $I_z = \frac{1}{2}$ and $I_z = \frac{3}{2}$ Ξ^* states. Altogether, higher-mass Ξ-resonance production in K^-n interactions at 2.87 GeV/c appears to be at or below the 5-μb level.

The absence of any $\Xi^-\pi^-$ resonance can be used to show conclusively that any Ξ resonances of mass less than about 2 GeV/c^2 observed in the reaction $K^-p \to \Xi^-\pi^+K^0$ must have isospin $\frac{1}{2}$ rather than $\frac{3}{2}$. From isospin coupling alone we have

$$\frac{\sigma(K^-n \to \Xi^{*--}_{3/2}K^+;\ \Xi^{*--}_{3/2} \to \Xi^-\pi^-)}{\sigma(K^-p \to \Xi^{*0}_{3/2}K^0;\ \Xi^{*0}_{3/2} \to \Xi^-\pi^+)} = 9 .$$

Thus a marginal $\Xi^*_{3/2}$ resonant signal of ~5 μb in $\Xi^-_1\pi^+K^0_1$ should appear as a huge peak of about 360 events in our $\Xi^-\pi^-$ mass distribution. This is inconsistent with the total of 238 events in the final state $\Xi^-\pi^-K^+$.

*Work supported by the Energy Research and Development Administration.

†Present address: Argonne National Laboratory, Argonne, Ill. 60439.

‡Present address: Digital Equipment Corporation, Maynard, Mass. 01754.

[1]In Greek mythology, Tantalus was punished for offenses to the gods by being hung from a tree and having food and water recede just beyond his reach whenever he grasped for them, for eternity. This seems to have a parallel in Ξ physics, where understanding appears to be always just as far away despite great experimental effort.

[2]A recent review of SU(3) assignments has been given by N. P. Samios, M. Goldberg, and B. T. Meadows, Rev. Mod. Phys. 46, 49 (1974).

[3]See, for example, R. H. Dalitz, in *Baryon Resonances—73*, edited by E. C. Fowler (Purdue, West Lafayette, Indiana, 1973), p. 393; R. Horgan, Nucl. Phys. B71, 514 (1974).

[4]S. Apsell *et al.*, Phys. Rev. Lett. 23, 884 (1969); S. Apsell *et al.*, *ibid.* 24, 777 (1970); R. J. Hemingway, BMST contribution to *Hyperon Resonances—70*, edited by E. C. Fowler (Moore, Durham, North Carolina, 1970), p. 317.

[5]For acceptance as a bona fide resonance candidate, a signal is usually required to have a significance of about 5 standard deviations. Historically this has been relaxed to about 3 standard deviations for Ξ studies. Our signals do not meet even this reduced requirement.

[6]D. J. Crennell *et al.*, Phys. Rev. D 1, 847 (1970).

[7]See, for example, G. C. Moneti, in *Baryon Resonances—73*, edited by E. C. Fowler (Purdue, West Lafayette, Indiana, 1973), p. 335, and references therein.

[8]T. Hamada and I. Johnston, Nucl. Phys. 34, 382 (1962).

[9]The commonly used Hulthén wave function [I. Hulthén and M. Sugawara, in *Encyclopedia of Physics*, edited by S. Flügge (Springer, New York, 1957), Vol 39] yields a correction factor of 0.94.

[10]R. Glauber, Phys. Rev. 100, 242 (1955); H. Braun *et al.*, Phys. Rev. D 2, 488 (1970).

[11]H. Geiger and A. Werner, Z. Phys. 21, 187 (1924).

[12]S. Derenzo and R. Hildebrand, Nucl. Instrum. Methods 69, 287 (1969).

[13]R. J. Hemingway and H. Whiteside, University of Maryland Technical Report No. 70-065, 1969 (unpublished).

[14]This upper limit and subsequent ones were calculated in the following way: A smooth curve representing the shape of the mass distribution as determined by phase space plus the reflections of any identifiable resonances was defined as the background. In the mass region containing the greatest number of events above background, a resonance was hypothesized to exist, with a "signal" given by the actual number of events less the background. For computation of an upper limit with 90% confidence, it was then assumed that the observed signal was the result of a 1.65-standard-deviation statistical fluctuation from a larger number of true resonant events.

[15]Fits consisting of $\Xi^*(1530)$, $\Sigma^*(1960)$, and phase space, with and without a $\Xi\pi$ resonance at a mass of about 1890 MeV/c^2, yield 10% $\Xi^*(1530)$ and 20% $\Sigma^*(1960)$ ($\Gamma \simeq 60$ MeV). Since the ΞK signal is doubtful (see text), we show in Fig. 5 the distributions corresponding to 10% $\Xi^*(1530)$ production plus phase space.

[16]Evidence for $\Xi(1630)$ can be found in Ref. 4 and R. T. Ross *et al.*, Phys. Lett. 38B, 177 (1972). For evidence against, see S. R. Borenstein *et al.*, Phys. Rev. D 5, 1559 (1972).